Measuring chromatic dispersion using single-arm interferometers: From millimeters to kilometers

Li Qian, Bing Qi, Waleed Mohammed[1], Michael Galle, Fei Ye
Department of Electrical and Computer Engineering, University of Toronto
10 King's College Road, Toronto, Ontario, Canada, M5S 3G4

ABSTRACT

We present three new interferometric techniques for dispersion characterization covering from millimeter waveguides to kilometers of fibers. The first is a Frequency-Shifted Interferometer (FSI) that measures fibers from meters to tens of kilometers. The second is a three-wave Single-Arm Interferometer (SAI), where the envelope of a three-wave interference pattern yields the second-order dispersion directly. It is suitable for fibers from centimeters to >1m. The third is a Common-Path Interferometer (CPI) that measures dispersion of millimeter-long fibers/waveguides. These techniques offer high precision in their respective ranges, and are all "single-arm" interferometers: the two interfering beams go through the same arm of the interferometer. They are simple, low-cost, and more resilient to phase and polarization instabilities than conventional interferometric techniques for dispersion measurement.

Keywords: Dispersion measurement, Frequency-Shifted Interferometer, Single-Arm Interferometer, Spectral interferogram, three-wave interference

1. INTRODUCTION

Chromatic dispersion of optical fibers and waveguides is an important design parameter for optical devices and systems. In linear systems, it can be the dominant factor in limiting the bandwidth of the system, and in nonlinear systems, it impacts directly the efficiency of the nonlinear interaction. Dispersion engineering can be used to either enhance or minimize the nonlinear effects. Therefore, determining the chromatic dispersion parameters accurately is essential in optical design.

This paper is devoted to the experimental techniques of accurately determining chromatic dispersion parameters of optical fibers and waveguides, covering a range of waveguide lengths, from millimeter-long nanowaveguides to kilometer-long optical fibers. The techniques introduced here are all interferometric in nature, and can in principle all be implemented with single-ended access using interferometers of a single arm (i.e., all interfering signals are going through the same arm of the interferometer). The single-arm interference provides simplicity and stability, and consequently, low-cost and accuracy, respectively.

1.1 Definitions of chromatic dispersion parameters

Chromatic dispersion arises from the wavelength dependence of the refractive index. In a waveguide, both material dispersion and waveguide dispersion contribute to the overall chromatic dispersion. The relationship between the effective mode index of a waveguide, n_{eff}, and the first, second and higher order dispersions can be understood mathematically through its Taylor expansion:

$$n_{eff} = n_{eff}(\lambda_o) + (\lambda - \lambda_o)\left.\frac{dn_{eff}}{d\lambda}\right|_{\lambda_o} + (\lambda - \lambda_o)^2\left.\frac{d^2 n_{eff}}{d\lambda^2}\right|_{\lambda_o} + (\lambda - \lambda_o)^3\left.\frac{d^3 n_{eff}}{d\lambda^3}\right|_{\lambda_o} + \ldots \quad (1)$$

where λ_o is the wavelength of interest. The first term in (1) relates to the phase velocity of the wave propagating in a waveguide, while the second term relates to the group velocity, $v_g(\lambda_o)$, and is called the first order dispersion, or linear dispersion. The group velocity is the velocity of the envelope of a pulse that has a finite bandwidth centered at λ_o. For

[1] Current address: International school of engineering, Chulalongkorn University, Bangkok, Thailand

Optics and Photonics for Information Processing II, edited by Abdul Ahad Sami Awwal, Khan M. Iftekharuddin, Bahram Javidi, Proc. of SPIE Vol. 7072, 70720D, (2008)
0277-786X/08/$18 · doi: 10.1117/12.795103

convenience, one can also define a group delay, $\tau_g(\lambda_o)$, which is the time it takes for the pulse to travel over a distance L in a waveguide. The third term in (1), also known as the quadratic or the second-order dispersion term, leads to the variation in the group velocity as a function of wavelength, known as Group Velocity Dispersion, GVD:

$$GVD(\lambda_o) = -\frac{\lambda_o^{\,2}}{2\pi c}\left[-\frac{\lambda_o}{c}\frac{d^2 n_{eff}}{d\lambda^2}\right] \tag{2}$$

The term in the brackets in Eq. (2) is defined as the group delay dispersion parameter, D:

$$D(\lambda_o) = -\frac{\lambda_o}{c}\frac{d^2 n_{eff}}{d\lambda^2}\bigg|_{\lambda_o} \tag{3}$$

The physical interpretation of D is the amount of group delay difference experienced over a unit wavelength spacing over a unit length:

$$D(\lambda) = \frac{1}{L}\left(\frac{d\tau_g}{\partial\lambda}\right) \tag{4}$$

Sometimes, linear and quadratic dispersions are expressed by the first and second derivatives of β with respect to wavelength, the propagation constant of the waveguides/fibers. GVD can be expressed by β' and β'' by

$$\mathrm{GVD} = \frac{\lambda^3}{(2\pi c)^2}\left(2\beta' + \lambda\beta''\right) \tag{5}$$

GVD, D, or β'' can be used to characterize the second-order chromatic dispersion, which is related to the pulse broadening that critically limits the bit rate of a communication system, as well as to the nonlinear interaction length in nonlinear devices. Hence, in many cases, the second-order dispersion is of the most importance when designing or analyzing photonic devices or systems, and measuring accurately the dispersion parameter of a variety of devices/systems becomes indispensable.

1.2 A brief review of various dispersion measurement techniques

Dispersion measurement techniques can be divided into two categories, those that measure long fibers (tens of meters to kilometers) and those that measure short fibers or waveguides (<1 meter). Long-length measurements are required on installed fiber spans or photonic components containing long lengths of fibers (such as a dispersion-compensating fiber module), whereas short-length measurements are required typically on waveguide devices (such as integrated lightwave circuits), gain fiber modules, and specialty fibers (such as photonics crystal fibers) where long lengths are either too expensive or not available. Additionally, when fiber uniformity changes significantly along its length, the dispersion of a long span of fiber cannot be used to accurately represent that of a short section of fiber. In such cases, dispersion measurement performed directly on short fiber samples is desirable.

The long-length category includes two of the most widely used commercial dispersion measurement techniques, the time of flight (TOF) technique [1] and the Modulation Phase Shift (MPS) technique [2, 3]. The TOF technique measures D by determining the relative temporal delay between pulses at different wavelengths. In the MPS technique, an optical signal is amplitude modulated by an RF signal and D is determined by measuring the RF phase delay, i.e., the delay in the wave envelope, at the different wavelengths. Measurement precision achievable by the TOF and MPS techniques are on the order of 1 ps/nm [2] and 0.07ps/nm [4], respectively. Due to its higher precision, MPS has become the industry standard method for measuring dispersion in optical fibers. However, MPS is expensive to implement and its precision is limited by both the stability and the jitter in the RF signal [5].

For short-length fiber/waveguide measurement, one has to employ interferometric techniques as the group delay is too small to be measured directly. There are two sub-categories of interferometric techniques: temporal and spectral. Temporal interferometry [6-8] employs a broadband source and a variable optical path to produce a temporal interferogram between a fixed path through the test fiber and the variable path. The spectral amplitude and phase are then determined from the Fourier transform of the temporal interferogram. The dispersion is indirectly obtained by

taking the derivative of the spectral phase. A precision of 0.0015 ps/nm measured on a 0.814-m-long photonic crystal fiber [8] was recently reported using temporal interferometry. The main disadvantage of temporal interferometry is that it is susceptible to noise resulting from both translation inaccuracy and vibration of the optics in the variable path. A tracking laser is typically required to calibrate the delay path length [7, 8].

Spectral interferometry [9-11] is generally more stable since the arms of the interferometer are kept stationary, and no tracking laser is necessary. In spectral interferometry, spectral fringes are produced by the interference of broadband light after propagating through two paths: one contains the test fiber and the other is a reference path containing a fixed delay. The spectral phase of the lightwave passing through the test fiber relative to that through the reference path can be extracted from the fringe pattern, and in principle, higher order dispersion can be derived. Alternatively, second-order dispersion can be measured directly (and therefore more accurately) by employing a balanced dual-arm interferometer [11] with an adjustable optical path in one arm. The adjustable arm is set to have the same group delay as the test fiber to remove the effect of the large linear dispersion in the interferogram. A precision of 0.00007 ps/nm has been reported on a SMF28^{TM} of 1m using this technique [11].

1.3 Dispersion measurements based on single-arm interferometers

To overcome the challenges and limitations presented in the above-mentioned dispersion characterization techniques, in this paper, we present three new interferometric techniques for dispersion characterization that cover the range from millimeter waveguides to kilometers of fibers. The first is based on a Frequency-Shifted Interferometer (FSI), suitable for measuring fibers from ~1m to tens of kilometers. The second is a three-wave Single-Arm Interferometer (SAI), where we use the envelope of a three-wave interference pattern to measure the second-order dispersion directly. It is suitable for fibers from a few centimeters to ~1m. The third is a Common-Path Interferometer (CPI) where dispersion can be measured on millimeter-long fibers/waveguides.

All three techniques utilize interferometry to achieve high precision in their respective measurement ranges. Moreover, all three are "single-arm" interferometers in that the interfering light signals go through the same arm of the interferometer. Compared to dual-arm interferometers, our systems offer fewer components, easier alignment, and less susceptibility to phase and polarization instabilities.

This paper is organized as follows: After the Introduction, we present the methods of FSI, three-wave SAI and CPI for dispersion characterization in Section 2, 3, and 4, respectively. We will elaborate on the principle of operation, experimental results, and discussions on the advantages and limitations of each method separately. In Section 5, we present our conclusion.

2. DISPERSION MEASUREMENT BASED ON FSI

In this section, we will introduce an interferometric technique for measuring linear and quadratic dispersion on long fibers. Unlike the TOF technique, this method requires only a cw source. Its implementation is much simpler and less expensive than the MPS technique.

2.1 Description of FSI and its principle of operation

An FSI consists of a loop interferometer, such as a Sagnac interferometer, and a frequency shift element which is placed in the loop asymmetrically [12]. Due to this asymmetry, counter-propagating light waves going through the loop will experience the frequency shift at different locations, resulting in a phase difference, which is related the amount of frequency shift and the relevant path length imbalance, and a corresponding interference signal results.

One of FSI's many applications [12-14] is chromatic dispersion measurement. The basic principle of using FSI for measuring chromatic dispersion can be understood from Fig.1. The input laser beam is split by a 50/50 coupler into two parts equally: a clockwise-propagating S_1 field and a counterclockwise-propagating S_2 field. The frequencies of both S_1 and S_2 are up-shifted by the same amount ($+f$) after they pass through the frequency shift element and a stable interference signal can be observed at the output port of the beam splitter. Since the frequency shift element is placed in the Sagnac loop asymmetrically, the phase delays experienced by S_1 and S_2 as they go through the loop could be different. Suppose the light frequency before and after going through the frequency shift element are ν_0 and ν' respectively, where $\nu'-\nu_0 = f$. The phase delays experienced by S_1 and S_2 can be expressed as

$$\Delta\phi = \phi_1 - \phi_2 = \left(k_{v_0} l_1 + k_{v'} l_2\right) - \left(k_{v_0} l_2 + k_{v'} l_1\right) = \left(l_2 - l_1\right)\left(k_{v'} - k_{v_0}\right)$$
$$= \Delta l \cdot \left.\frac{dk}{dv}\right|_{v_0} \cdot dv = \Delta l f \cdot \left.\frac{dk}{dv}\right|_{v_0} \tag{6}$$

where k_v is the propagation constant as a function of frequency, and $\Delta l = l_2 - l_1$ is the path length imbalance. $\Delta\phi$ is related to the group delay τ_g by:

$$\tau_g = \frac{L}{V_g} = \frac{L}{2\pi}\frac{dk}{dv} = \frac{L}{2\pi}\frac{\Delta\phi}{\Delta l f} \tag{7}$$

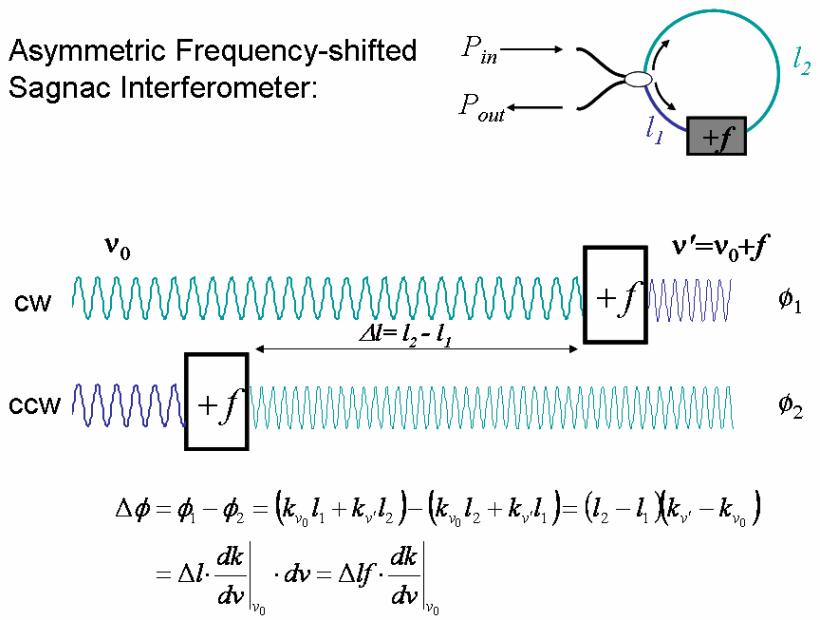

Fig.1. The conceptual structure and the principle of operation of a Sagnac FSI.

The interference signal, which is given by $V \propto \cos(\Delta\phi)$, is a periodic function of f. By scanning f while recording V, the group delay τ_g can be determined from the "period" of V with a high resolution. Therefore, the linear dispersion can be obtained directly. If τ_g is measured over wavelength, the second-order dispersion can be obtained by taking the derivative of τ_g with respect to wavelength as indicated in Eq. (4).

2.2 Experimental results and discussions

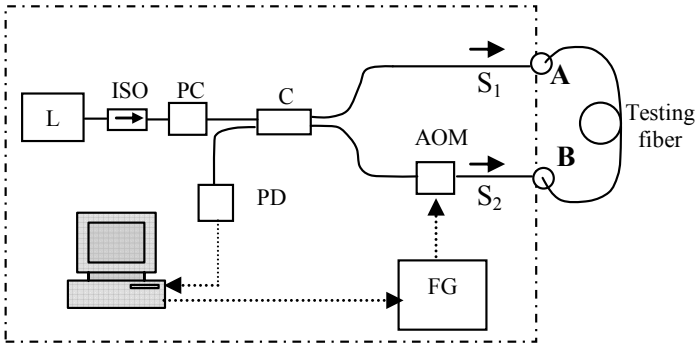

Fig.2. Frequency-shifted interferometer for fiber dispersion measurement: L—tunable laser; ISO—isolator; PC—polarization controller; C—2x2 50/50 fiber coupler; AOM—acousto-optic modulator; FG—function generator; PD—photo detector.

Fig. 2 shows our experimental setup. Here, a polarization insensitive fiber-pigtailed acousto-optic modulator (AOM, Brimrose Corp.) was used to achieve the frequency shift. Its driving signal is provided by the output of a function generator, and is linearly swept over time. A CW tunable laser is used as the light source. A polarization controller is employed to improve the visibility of the interference signal. To obtain the group delay $\tau_g(\lambda)$ over wavelength, the wavelength of the tunable laser is swept. At each laser wavelength, by scanning the driving frequency of AOM while recording the interference signal, the group delay at this specific wavelength can be determined.

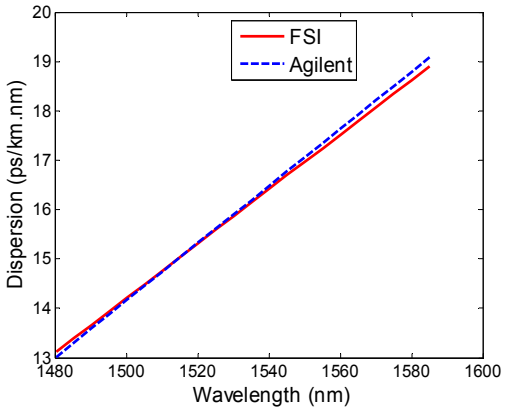

Fig.3. Chromatic dispersion measurement for a 20km SMF-28: Solid line—FSI system; Dashed line—Agilent 86037C Chromatic Dispersion Test system (MPS).

We performed dispersion measurement over the range of 1480-1585nm on a 20km SMF28^{TM} fiber spool using the FSI technique. Fig. 3 shows a comparison between the dispersion result obtained from our FSI system and that from an Agilent 86037C Chromatic Dispersion Test system, with uses the MPS technique. The slight discrepancy may be attributed to the wavelength dependence of the components in the FSI system, which was not calibrated.

Compared with conventional techniques for measuring dispersion over long fibers, using FSI to measure chromatic dispersion is simple, cost effective and robust. The system can be constructed by a CW laser source in combination with a low-speed photo detector. It provides stable interference even for long spools of fiber (tens of kilometers), since the two interfering signals go through the same optical path, eliminating phase instabilities due to environmental disturbances. Polarization instability, though cannot be eliminated, can be reduced through passive means to such a degree that the system remains stable over the measurement time. Also, since the group delay is related to the *phase* of the interference signal while polarization change affects the *amplitude*, polarization instability has much less significance on the measurement result.

While the FSI method is accurate for long spools of fiber, its accuracy starts to suffer as fiber length shortens. Since this method does not measure the second-order dispersion directly, a relative error of less than 10^{-4} is typically required for the linear dispersion measurement in order to achieve an error of less than a few percent on the second-order dispersion. This limits the minimum length that can be measured accurately to be a few meters [12]. In addition, for short length measurement, a long compensating fiber [12] is required. In this case, the dispersion of the compensating fiber will need to be calibrated.

Though our experiment was carried out in a Sagnac FSI, it can be easily re-configured into a folded Mach-Zehnder FSI [13, 14] which requires only one-ended access to the fiber under test.

3. DISPERSION MEASUREMENT BASED ON THREE-WAVE SAI

In this section, we will introduce a technique that measures the dispersion on short lengths of fibers/waveguides. Since it is actually the dispersion-length (*DL*) product that is measured, it is particularly challenging when the measurand, that is, the *DL* product, becomes small. Spectral interferometry is employed here. But unlike the conventional dual-arm interferometer, we construct a single-arm interferometer to avoid some of the pitfalls in the conventional techniques.

3.1 Balanced dual-arm interferometer versus the three-wave SAI

A balanced dual-arm interferometer, either in a Mach-Zehnder or a Michelson configuration, is traditionally employed for second-order dispersion measurements on short lengths of fibers/waveguides. In the balanced Michelson interferometer set up (Fig. 4(a)), a spectral interferogram is created from the reflections at the ends of the two paths, U_1 (in the reference path) and U_2 (in the test path), as shown. The dispersion parameter D of the test path can be obtained directly if the dispersion of the reference path is known and if the group delays of the two paths are made equal at the wavelength of interest.

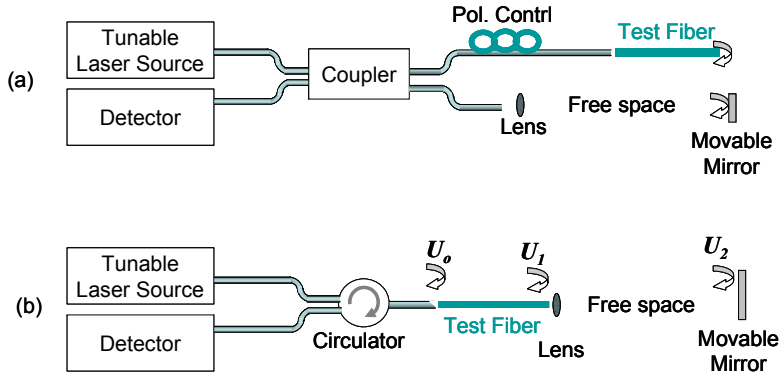

Fig. 4: (a) A conventional fiber-based Michelson interferometer (i.e., a two-wave dual-arm interferometer) and (b) a fiber-based three-wave single-arm interferometers for dispersion measurement

For a fiber-based dual-arm interferometer, several practical problems arise. First, there are undesirable interference fringes created by the reflections from the two end facets of the coupler fiber leads, which can distort the spectral interferogram created by U_1 and U_2. To avoid this, the two coupler leads are intentionally made to have a large length difference so that the undesirable fringes are "fast" varying and can be eliminated by a low-resolution spectrometer. However, this creates a second problem, that is, the dispersion of the lead fibers must be calibrated out, and the calibration step will introduce additional measurement error, which can be significant especially when the DL product of lead fibers is comparable to or larger than that of the test fiber, which is often the case. Third, as the two interfering signals travel down two different fiber paths, experiencing different environmental disturbances, causing phase and polarization instabilities which would impact the accuracy of the results significantly.

To avoid these drawbacks, here we present an SAI, where interfering signals travel in the same "arm" of the interferometer. The set up is shown in Fig. 4(b). The core of the SAI consists of two components, an air path and a fiber. There are three 'in line' reflections in an SAI. Two reflections come from the front and end facets of the test fiber (U_0 and U_1) and one reflection comes from the mirror placed at the end of the air path (U_2). (One can also arrange in such a way that the air path precedes the test fiber.) These three reflections are made to interfere, generating a three wave interference pattern. Since the SAI configuration has no coupler and no path spliting of the light, there is no need for calibration of the fiber leads and hence eliminating the uncertainties introduced into the measurements during the calibration. The SAI also suffers less from phase and polarization instabilities due to environmental disturbances. Therefore, it is capable of characterizing smaller DL products with higher accuracy than with a dual arm interferometer.

3.2 Principle of operation

The interference pattern produced by the three interfering waves can be expressed as [15]:

$$\begin{aligned} I_o &= \left|U_0 + U_1 + U_2\right|^2 = U_0^2 \left|1 + a e^{-i2\beta L_f} + b e^{-i2\beta L_f - i2k_o L_a}\right|^2 \\ &= U_0^2 \left\{1 + a^2 + b^2 - 2b + 4b\cos^2\left(\beta L_f + k_o L_a\right) + 2a(1-b)\cos\left(2\beta L_f\right)\right. \\ &\quad \left. + 4ab\cos\left(\beta L_f + k_o L_a\right)\cos\left(\beta L_f - k_o L_a\right)\right\} \end{aligned} \tag{8}$$

where L_f and L_a are the lengths of the fiber path and the air path, respectively. β and k_o are the propagation constant of the fundamental fiber mode and that of the free space, respectively. a and b are the relative amplitudes of U_1 and U_2, respectively, with respect to U_0. The interference pattern expressed by (8) has a few "fast-varying" terms, all are

modulated by a "slow-varying" envelope with a phase evolution $\phi_{envelope} = \beta L_f - k_o L_a$. A simulated interference pattern is shown in Fig. 5. When b is large (>0.5), it can be shown [15] that the upper envelope is approximated by:

$$U_o^2\left(1+a^2+b^2+2a(b-1)+2b+4a\left|\cos(\phi_{envelope})\right|\right) \tag{9}$$

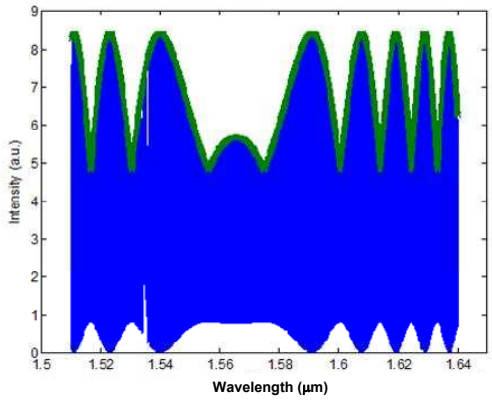

Fig. 5: Simulated interference pattern (blue) produced using a three-wave SAI for a 30-cm SMF28TM Fiber, with a=0.9 and b =1. The individual fringes are two dense to be resolved visually here. The envelope function calculated by Eq. (9) is superimposed on the interferogram as the thick green line.

If we replace β with $2\pi n_{eff}/\lambda$ and Taylor expand the phase of the envelope $\phi_{envelope}$, we obtain:

$$\phi_{envelope}(\lambda) = 2\pi\left\{\frac{1}{\lambda}\left[\left(n_{eff}(\lambda_o)-\lambda_o\left.\frac{dn_{eff}}{d\lambda}\right|_{\lambda_o}\right)L_f - L_a\right] + L_f\left.\frac{dn_{eff}}{d\lambda}\right|_{\lambda_o} + L_f\frac{(\lambda-\lambda_o)^2}{2!\lambda}\left.\frac{d^2n_{eff}}{d\lambda^2}\right|_{\lambda_o} + L_f\frac{(\lambda-\lambda_o)^3}{3!\lambda}\left.\frac{d^3n_{eff}}{d\lambda^3}\right|_{\lambda_o} + \cdots\right\} \tag{10}$$

If the group delay in the air path balances that in the test fiber at a given wavelength λ_o, then the first term in (10) disappears. The envelope phase difference at two separate wavelengths, λ_1 and λ_2, that correspond to two peaks (or two troughs) of the envelope is:

$$\begin{aligned}\Delta\phi_{envelope} &= \left|\phi_{envelope}(\lambda_2)-\phi_{envelope}(\lambda_1)\right| \\ &= 2\pi\left(\left[\frac{(\lambda_2-\lambda_0)^2}{2!\lambda_2}-\frac{(\lambda_1-\lambda_0)^2}{2!\lambda_1}\right]\left.\frac{d^2n_{eff}}{d\lambda^2}\right|_{\lambda_0} + \left[\frac{(\lambda_2-\lambda_0)^3}{3!\lambda_2}-\frac{(\lambda_1-\lambda_0)^3}{3!\lambda_1}\right]\left.\frac{d^3n_{eff}}{d\lambda^3}\right|_{\lambda_0}\right)L_f \\ &= m\pi\end{aligned} \tag{11}$$

where m is the number of fringes between the two wavelengths. If this phase difference is taken using a two pairs of peaks/troughs (e.g., λ_1 & λ_2, and λ_{-1} & λ_{-2}), the result is a system of equations in which $\left.\frac{d^2n_{eff}}{d\lambda^2}\right|_{\lambda_o}$ and $\left.\frac{d^3n_{eff}}{d\lambda^3}\right|_{\lambda_o}$ can be solved directly [11]. Note that, if we ignore the third-order dispersion, then only one pair of wavelengths (e.g., λ_1 & λ_2) are required to calculate the second-order dispersion; however, it would be less accurate. The dispersion parameter D can then be found using Eq (3).

3.3 Measurement results

We will show our experimental results on the measurements of D on two short fibers: a 39.5-cm long SMF28^{TM} (Fig. 6), and a 15.5-cm long Dispersion Compensating Fiber (DCF) (Fig. 7). The results are compared to either simulated dispersion curves using published data or measured dispersion curves using an alternative technique.

The standard deviation of the points measured on SMF28^{TM} using SAI (Fig. 6) is calculated to be 0.28 ps/nm-km (corresponding to a relative error of 1.6%). Multiplying the standard deviation by the fibre length translates into a

standard deviation of 0.0001 ps/nm. Note that this precision is obtained from the raw measurement data, without any curve fitting. Yet, the 1×10^{-4} ps/nm precision obtained here on a 40-cm SMF using the three-wave SAI is comparable to the 7×10^{-5} ps/nm precision obtained with curve fitting on a 1-m long SMF using a two-wave dual-arm balanced interferometer [11].

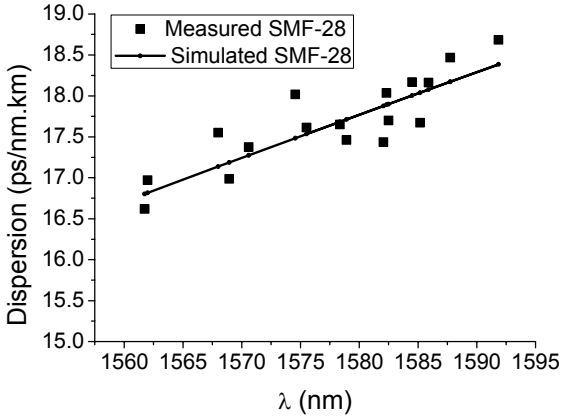

Fig. 6: Measured dispersion (squares) compared to calculated dispersion using published data (line) for a 39.5+0.1cm SMF28^{TM} fiber.

The measured dispersion on the 15.5-cm long DCF (Fig. 7) has a standard deviation (calculated by taking the difference between the measured points and a linear fit) of 0.99 ps/nm-km, which corresponds to a relative error of 0.9%. When multiplied by the length of the fiber, this translates into a precision of 0.00015 ps/nm. The measured *D* agrees very well with the measurement given by a commercial dispersion measurement instrument (Agilent 83427A) which employs the MPS technique. Note, we achieved similar accuracy in measured *D* on a fibre that is three orders of magnitude shorter than that was used on the commercial instrument.

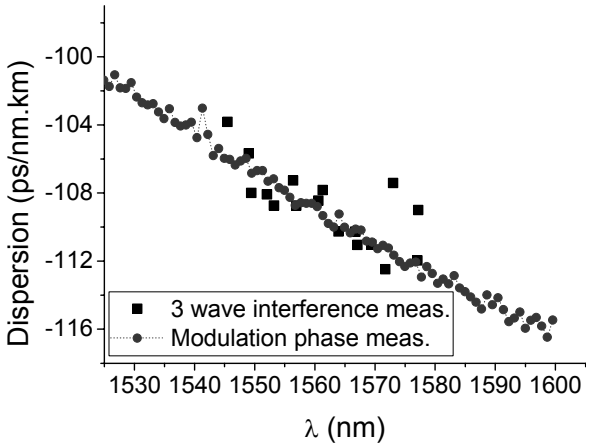

Fig. 7: Measured dispersion data on a DCF using SAI (squares) compared to those measured by Agilent 83427A. The length of the fiber used in the SAI experiment was 15.5 cm while the length of fiber used by Agilent was 100 m.

3.4 Discussions

We have demonstrated that three-wave SAI can perform accurate second-order dispersion measurements on short fibers, with a *DL* product in the range of 10^{-2}ps/nm, with a precision of 1×10^{-4}ps/nm. In this section, we will quantify the measurement range and resolution of this technique. The parameters that characterize this technique are: the wavelength resolution of the measurement, the minimum required source bandwidth, the measurable bandwidth of the dispersion curve, the minimum *DL* product, and the maximum fiber length.

The wavelength resolution $\delta\lambda$ of the three-wave SAI measurement is limited by the length resolution of the air path, δL_a, and is given by [15]:

$$\delta\lambda = \frac{1}{cDL_f}\delta L_a \tag{12}$$

The minimum required source bandwidth is the smallest bandwidth required to capture enough (envelope) interference fringes. The smallest bandwidth must include the balanced wavelength and at least four other peaks or troughs of the envelope fringes (referring to Fig. 5). Using this reasoning, it can be determined that the lower bound on the required bandwidth, in the same unit as the wavelength, is given by [15]:

$$B_{\min} = 2\sqrt{2}\frac{\lambda_0}{\sqrt{cDL_f}} \tag{13}$$

The measurable bandwidth, B_{mea}, of the dispersion curve should be the difference between the actual bandwidth of the source and the minimum required source bandwidth, B_{min}, and therefore:

$$B_{mea} = B_{source} - B_{\min} \geq B_{source} - 2\sqrt{2}\frac{\lambda_0}{\sqrt{cDL_f}} \tag{14}$$

It can be seen clearly that the *DL* product impacts the system parameters, and, for a given system, the minimum DL product is limited by the wavelength resolution requirement, or by the required measurement bandwidth, and by the source bandwidth. As a minimum requirement, $B_{mea} = B_{source} - B_{min} \geq 0$. Therefore, for a given source bandwidth, the *DL* product must meet:

$$DL_f \geq \frac{8\lambda_o^{\,2}}{cB_{source}^{\,2}} \tag{15}$$

For example, if the source bandwidth is 100 nm, then the minimum *DL* product for second-order dispersion to be accurately measured at 1.55um is 6.4×10^{-3} ps/nm.

As the three-wave SAI technique relies on the envelope of the interference fringes, one requires in general that the individual fringes be adequately resolved. This imposes a maximum limit on fiber length, as an increase in fiber length results in narrower fringe spacing. As a result, the wavelength resolution of the tunable laser ($\Delta\lambda$) sets a limit on the maximum fiber length:

$$L_f \leq \frac{\lambda_o^{\,2}}{4n_{eff}\,\Delta\lambda} \tag{16}$$

This length, however, can be overcome by the process of wavelength windowing which uses a tunable laser source with random step size and plots the envelope by taking the maximum in a given wavelength range [16].

In short, within the limits set out by the system parameters (Eq (13)-(15)), the three-wave SAI technique is a simple, stable, and accurate technique for characterizing the second-order chromatic dispersion in fibers and waveguides. For fibers/waveguides with a *DL* product smaller than the limit set out by Eq (15), we will introduce another single-arm interferometer technique in the next section.

4. DISPERSION MEASUREMENT BASED ON CPI

This section presents a simple common-path interferometric (CPI) technique to measure linear and quadratic dispersion parameters on specialty fibers, waveguides, and nano-wires, which are millimeters in length. Our technique is based on extremely accurate measurement of linear dispersion from the spectral Fabry-Pérot fringes generated by the reflections from both facets of the sample. The high accuracy is achieved using a moving spectral window, and the linear dispersion at the central wavelength of the window is obtained using Fourier analysis. As a result, measurement precision of 1.45×10^{-4} is achieved on linear dispersion, which allows for accurate extraction of the quadratic dispersion.

4.1 Principal of operation

The essential element of this technique is to rely on the highly precise measurement of the linear dispersion so that higher order dispersion parameters can be extracted accurately. The experimental setup (Fig. 8) consists of a broadband source, a circulator, and the cleaved sample under test. Light from the broadband source is launched into the sample through the circulator and an angle-cleaved connector, which eliminates the reflection from the connector-air interface. The Fabry-Pérot interference fringe pattern produced by multiple reflections from both facets of the sample is recorded on the optical spectrum analyzer (OSA). One can also use transmission instead of reflection.

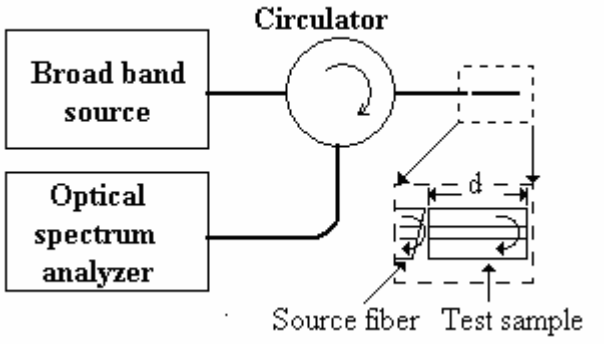

Fig. 8 The experimental setup of the single-arm interferometer for measuring the dispersion of fibers waveguide samples.

In order to extract as accurately as possible the linear dispersion parameter, β', defined as the first derivative of the propagation constant with respect to wavelength, we divide the total bandwidth into a number of overlapping wavelength windows (subbands), and assume a fixed fringe period in each subband. This assumption is valid when $\Delta\lambda_j << \frac{2\beta'(\lambda_j)}{\beta''(\lambda_j)}$, where $\Delta\lambda_j$ and λ_j are the width and the center wavelength of the j[th] subband, respectively. Under this assumption, β' at λ_j can be found using Fourier analysis. Fourier series expansion of the normalized Fabry-Pérot intensity gives a series of peaks and β_j' can be measured directly from the index of the first peak, $m_{p,j}$, as follows,

$$\beta_j' = \frac{\pi m_{p,j}}{\delta\lambda M d} \tag{17}$$

where M is the total number of samples in the Fourier domain and $\delta\lambda$ is the wavelength sampling step. This method returns β' across the total wavelength range with a coarse wavelength resolution that equals the separation between the centers of the subbands. β'' at each wavelength, λ_j, is calculated by fitting $\beta'(\lambda)$ to a second order polynomial around λ_j and $\beta''(\lambda_j)$ equals the linear term coefficient.

4.2 Experimental results and discussions

We used this method to measure the dispersion parameters on three samples: a 6 mm long twin-hole fiber, a 2.88 mm long AlGaAs waveguide and a set of $Al_{0.2}Ga_{0.8}As$ nano-wires of various widths and lengths. The twin-hole fiber sample consisted of a 4.5-μm radius Ge-doped silica core between two 45 μm radius air holes. The waveguide consisted of a 1.5 μm $Al_{0.18}Ga_{0.82}As$ core layer, surrounded by $Al_{0.24}Ga_{0.76}$ cladding layers (1.5 μm above, and 4.0 μm below), grown on a GaAs substrate with a 3.5-μm-wide and 2-μm-deep ridge. The nanowires samples had lengths of 0, 300, 600, and 1000 μm, and the core height is 500nm. The wires were feed by a 2 μm wide waveguide and a 150 μm long taper. The full structure was 2.4 mm long.

To estimate the validity limit of the subband window, we need to estimate β' and β''. For the fiber sample, we used the published D and group index values of the SMF28[TM] fiber. For waveguides/nano-wires samples, we used the effective index method to estimate β' and β''. As a result, the estimated maximum subband width is 4.17 nm for the fiber sample, and 11.85 nm for the waveguide and nanowires. Hence, in all the measurements we chose a 3 nm sub-band width.

The sources used in our measurements were an erbium-doped-fiber ASE source (50 nm bandwidth) for the twin-hole fiber, and an Agilent 83437A broadband source (250 nm) for the waveguide sample and nano-wires. For all cases, we

found there was no need for phase stabilization during measurement. The average fringe period L_j of each subband is measured using a peak finding technique after smoothing the data (moving average).

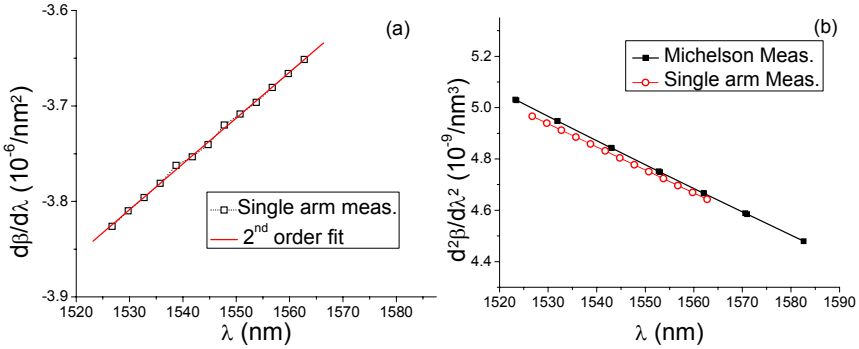

Fig. 9. Measured β' (a) and β'' (b) on a 6-mm piece of twin-hole fiber using the single-arm CPI method. The measured β'' is compared to the values measured using a dual-arm Michelson interferometer on a 10-cm piece of the same fiber.

The plots in Fig. 9 depict the measured β' and β'' for the twin-hole fiber using the Fourier analysis. These results show a good agreement (difference less than 0.45%) with those obtained from balanced Michelson interferometer measurements with a 10 cm piece of the same fiber.

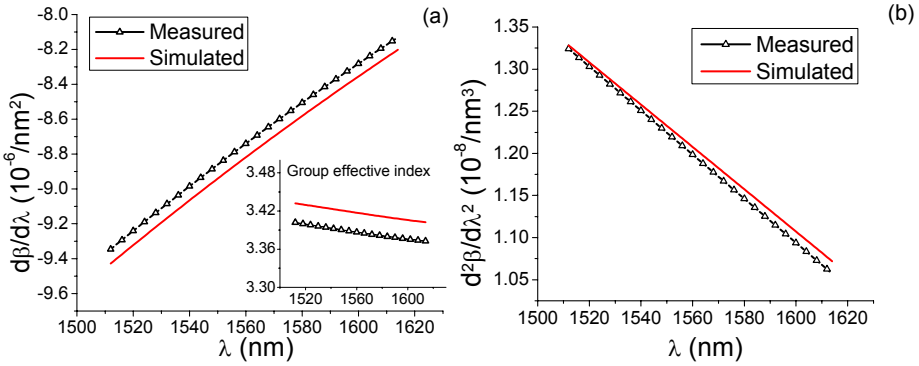

Fig. 10. (a) Measured β' and group index (inner graph) and (b) β'' compared to the simulated dispersion for a 2.88 mm AlGaAs ridge waveguide sample using effective index method.

Fig. 10 shows the measured β' and β'' on the AlGaAs waveguide sample, in comparison with the simulated dispersion using the effective index method [17]. The measured dispersion parameters show a good agreement with the simulated dispersion with discrepancies of less than 0.9%, which can be attributed to the uncertainties in the simulation parameters. The D and GVD values calculated from β' and β'' using Eq. (5) at 1550 nm are –1036.5 ps/nm.km and 1.32 ps^2/nm respectively, which are close to the reported bulk $Al_{0.2}Ga_{0.8}As$ parameters (|D|=1000 ps/nm.km and GVD=1 ps2/nm) [18]. The differences are due to waveguide dispersion and the core material being slightly different from that is used in ref. 18 ($Al_{0.18}Ga_{0.82}As$).

Finally, we applied our technique to AlGaAs nanowires and demonstrated that this structure exhibits strong GVD inversion for submicron wide waveguides for the first time [19], which has been recently predicted theoretically [20]. We used nanowires of various lengths in order to calibrate out the dispersion of the feed waveguides and the tapers. The measured results are shown in Fig. 11 together with the theoretically calculated values. For waveguide widths between 670 nm and 281 nm, the strong field confinement dominates the material dispersion and leads to an inversion of the GVD of the TE mode, as shown by both calculated and measured results. Here, the vertical error bars of the measured data points have been obtained by bootstrapping the measured fringe periods.

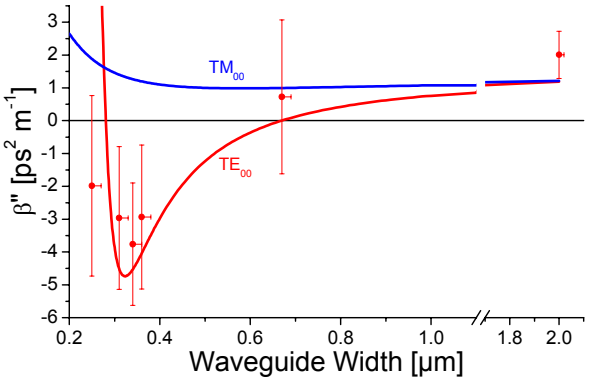

Fig. 11: Measured (dots with error bars) and calculated GVD vs. waveguide width at the wavelength of 1.55 μm.

It can be seen that this method can be fairly accurate, even for mm-length waveguides. The measured values of the linear dispersion β' have a standard deviation of 0.017% for the fiber sample, and 0.014% for the waveguide samples. The relative precision in the quadratic dispersion depends on the β'' value. For the fiber sample, the precision is <1%.

The main advantage of this technique is the fact that it can be applied to very short devices (mm length or even less). As fiber probe is used, the dispersion can be measured without the need to remove the desire waveguide from the setup. The main drawback of this method is the fact that precise measurement of the spectrum is needed, hence small resolution is used together with noise reduction scheme in order to minimize the error. Hence measurement time can be long (a few hours).

5. CONCLUSION

Chromatic dispersion is a key parameter in high-speed photonic systems as it affects pulse broadening and nonlinear optical processes. Dispersion engineering is required for a variety of systems, from long-haul communication spanning hundreds of kilometers to compact photonic circuits employing semiconductor nanowires or photonic crystal fibers. Accurate dispersion characterization is critical to the design of these systems. In the preceding sections, we presented three new techniques for dispersion characterization that cover the range from millimeter waveguides to kilometers of fibers. Experimental demonstrations were given for all three cases, and we have demonstrated that the accuracy of our techniques is comparable or exceeds that of conventional techniques. We have also pointed out the limitations and the validity range of our techniques.

All three techniques are interferometric in nature, hence offering high precision in their respective measurement range. Furthermore, their simple configurations facilitate alignment and are robust and inexpensive to implement. Moreover, to overcome the phase and polarization instabilities that are the major concerns in all fiber-based interferometers, all three techniques have the "single-arm" configuration such that the interfering signals go through the same arm of the interferometer, effectively eliminating/minimizing phase and polarization instabilities.

REFERENCES

[1] J. H. Wiesenfeld and J. Stone, "Measurement of dispersion using short lengths of an optical fiber and picosecond pulses from semiconductor film lasers," IEEE J. Lightwave Technol., 2, 464-468 (1984).

[2] L. G. Cohen. "Comparison of single-mode fiber dispersion measurement techniques,"IEEE J. Lightwave Technol., 3, 958-966 (1985).

[3] B. Costa, D. Mazzoni, M. Puleo, E. Vezzoni, " Phase Shift Technique for the measurement of Chromatic Dispersion in Optical Fibers using LED's", IEEE Transactions on Microwave Theory and Techniques, 82(10), 1497-1503 (1982)

[4] Agilent White Paper, "Agilent 86038B Photonic Dispersion and Loss Analyzer", http://cp.literature.agilent.com/litweb/pdf/5989-2325EN.pdf, (2007)

[5] L. Cherbi, M. Mehenni, and R. Aksas, "Experimental Investigation of the Modulation Phase-Shift Method for the Measure of the Chromatic Dispersion in a Single-Mode fiber coiled on a cover spool," Microwave and Opt. Technol. Letts. 48, 174-178 (2006)
[6] R. K. Hickernell, T. Kaumasa, M. Yamada, M. Shimizu, M. Horiguchi. "Pump-induced dispersion of erbium-doped fiber measured by Fourier-transform spectroscopy", Opt. Lett., 18(1), 19-21(1993)
[7] J. Gehler and W. Spahn, "Dispersion measurement of arrayed-waveguide grating by Fourier transform spectroscopy," Electron. Lett., 36, 338-340 (2000)
[8] C. Palavicini, Y. Jaouën, G. Debarge, E. Kerrinckx, Y. Quiquempois, M. Douay, C. Lepers, A.-F. Obaton, G. Melin, "Phase-sensitive optical low-coherence reflectometry technique applied to the characterization of photonic crystal fiber properties," Optics Letts., 30, 361-363 (2005)
[9] J. Tignon, M. V Marquezini, T. Hasch, and D. S. Chemals, "Spectral interferometry of semiconductor nanostructures," IEEE J. Quantum Electron., 35, 510-522 (1999)
[10] C. D. Dorrer, N. Belabas, J. P. Likforman, and M. Joffre, "Spectral resolution and sampling in Fourier transform spectral interferometry," J. Opt. Soc. Am. B, 17, 1795-1802 (2000)
[11] P. Merrit, R. P. Tatam, and D.A. Jackson, "Interferometric chromatic dispersion measurements on short lengths of Monomode optical fiber," J. Lightwave Technol. 7, 703-716 (1989)
[12] B. Qi, A. Tausz, L. Qian, and H-K. Lo, "High-resolution, large dynamic range fiber length measurement based on a frequency-shifted asymmetric Sagnac interferometer," Opt. Lett., 30(24), 3287-3289, (2005).
[13] B. Qi, L. Qian, A. Tausz, and H-K. Lo, "Frequency-shifted Mach-Zehnder interferometer for locating multiple weak reflections along a fiber link," IEEE Photon. Technol. Lett.,18(1), 295-297, (2006).
[14] Fei Ye, Li Qian, Yu Liu, and Bing Qi "Using Frequency-Shifted Interferometry for Multiplexing a Fiber Bragg Grating Array,", IEEE Photonics Technology Letters, Accepted (2008)
[15] M.A. Galle, W. S. Mohammed, L. Qian and Peter W. E. Smith, "Single-arm three-wave interferometer for measuring dispersion of short lengths of fiber" Opt. Express, 15, 16896-16908 (2007)
[16] M.A. Galle, "Single-arm three wave interferometer for measuring dispersion in short lengths of fiber", Thesis, University of Toronto, 2007
[17] M. Asobe, K. Naganuma, and T. Kaino, "Switching energy limitation in all-optical switching due to group velocity dispersion of highly nonlinear optical waveguides," App. Phys. Lett., 64, 2922-2924 (1994).
[18] K. Naganuma, "Semiconductor laser cavity dispersion measurement based on interferometric cross-correlation of amplified spontaneous emission," App. Phys. Lett. 64, 261-263 (1994).
[19] J. Meier, W.S. Mohammed, A. Jugessur, L. Qian, M. Mojahedi, J.S. Aitchison, "Group Velocity Inversion in AlGaAs Nanowires", Opt. Express, 15, 12755-12762 (2007)
[20] R. A. El-Ganainy, S. Mokhov, K. G. Markis, D. N. Christodoulides, "Solitons in dispersion-inverted AlGaAs nanowires," Opt. Express, 14, 2277 (2006)